Evolution of mushroom-type structures behind a heated cylinder

Evolution of mushroom-type structures behind a heated cylinder

Maosheng Ren,[a] Camilo Rindt, and Anton van Steenhoven
Laboratory for Energy Technology, Department of Mechanical Engineering,
Eindhoven University of Technology, P.O. Box 513, 5600 MB Eindhoven, The Netherlands

(Received 5 September 2006; accepted 18 April 2007; published online 27 June 2007)

The three-dimensional transition in the wake flow behind a heated cylinder occurs at a much lower Reynolds number than for the unheated case. The three-dimensional transition is initialized in the near-wake by the formation of Λ-shaped structures and manifests itself in the far-wake as escaping mushroom-type structures from the upper vortices. In this study, both experimental and numerical techniques are used to investigate the origin and development of these mushroom-type structures. The formation of the mushroom-type structures is associated with the occurrence of Λ-shaped vortices in the near-wake. Hot fluid between the legs and the head of the Λ-shaped structure is lifted up. This lift-up process together with the action of buoyancy pulls out hot fluid from the upper vortex cores, resulting in a mushroom-type structure, which is comprised of a so-called stem and cap. Hot fluid is continuously transported through the stem to the advancing front of the mushroom-type structure. Finally, a pinch-off phenomenon is observed of the cap, ending up as a buoyant vortex ring. An analytical model is presented for the pinch-off process. © *2007 American Institute of Physics*. [DOI: 10.1063/1.2741397]

I. INTRODUCTION

The aim of the present study is to investigate both experimentally and numerically the escaping mushroom-type structures in the far-wake of a heated cylinder for a relatively low Reynolds number. The wake instability behind an unheated cylinder has been the subject of many studies over more than a century. Several decades ago there was a renewed interest in this classical problem due to the ever growing computer resources and the sophisticated experimental techniques available nowadays, which can be used in understanding the details of the transition process and the route to turbulence for wake flows.

In Williamson,[1] an overview is given of the different features of the wake flow behind a cylinder for the forced convection case. For $\mathrm{Re}<50$, the wake consists of two counter-rotating vortices. The length of the recirculation zone grows as the Reynolds number increases. For $50<\mathrm{Re}<190$, the wake flow is characterized by alternately shed vortices. The onset of the wake instability near $\mathrm{Re}=50$ has been found to be a Hopf bifurcation (Provansal *et al.*[2]). The wake oscillations are purely periodic within this Reynolds range if parallel vortex shedding takes place. For $190<\mathrm{Re}<250$, a three-dimensional transition takes place (Williamson[3]). First the primary vortices deform in a wavy fashion along their length during the shedding process. This results in the local spanwise formation of vortex loops, which become stretched into streamwise vortex pairs. The spanwise length scale of these structures is typically four cylinder diameters. This is known as the mode-A of instability.

For slightly higher Reynolds numbers, a gradual transfer of energy takes place from the mode-A to a mode-B of instability, which is characterized by finer-scale streamwise vortex pairs with a spanwise length scale of typically one cylinder diameter. The process of transition is complicated by the existence of vortex dislocations (Williamson[4]). At these dislocations, the primary vortices seem to adhere at a steady or slowly moving point at the cylinder wall for many periods. This mode is referred to as the vortex-adhesion mode (Zhang *et al.*[5]). By placing an external interference, a thin wire, at suitable locations in the near wake, they also showed the existence of a so-called mode-C in water channel experiments and numerical calculations. The corresponding three-dimensional spanwise pattern has a wavelength of approximately 1.6 times the cylinder diameter.

Despite the fact that mixed convection around bluff bodies is of great importance for various engineering applications (electronics cooling, compact heat exchangers), wake instability for a heated cylinder has until now received very little attention compared to the forced convection case. Most previous studies were focused on the first transition from a two-dimensional steady to a two-dimensional periodic wake (or vice versa). It was observed that buoyancy tends to decrease the unsteadiness in the wake, finally leading to full suppression of the vortex street (Michaux-Leblond and Bélorgey,[6] Chang and Sa[7]) or tends to increase the unsteadiness in the wake (Hatanaka and Kawahara[8]), depending on the attack angle of the main flow with respect to the gravitational force. Mi and Antonia[9] studied the temperature distribution within vortices in the wake of a cylinder and concluded that this distribution is quite well approximated by the theoretical distribution for a diffusing line vortex. Ezersky and Ermoshin[10] studied the instability of a solitary vortex whose core has a lower density than the surrounding fluid. It is shown that for a vortex with an increasing density from the rotation axis to the periphery, flexural oscillations may be

[a]Present address: Oce-Technologies B.V. Research and Development, P.O. Box 101, St. Urbanusweg 43, 5900 MA Venlo, The Netherlands. Electronic mail: maosheng.ren@oce.com

excited. However, they did not take into account gravity effects.

The influence of heat input on the transition process toward three-dimensional coherent structures where buoyancy should be taken into account (Ri > 0.1) has not yet been investigated, until the recent studies performed in Refs. 11–17. For the forced convection case, the flow becomes three-dimensional for Reynolds numbers larger than Re=180. However, for the mixed convection case, the three-dimensional transition occurs at much lower Reynolds numbers (down to Re=85 for Ri=1.0 and water as the working fluid), which is referred to as the "mode-E" transition.[15] This three-dimensional transition is initialized in the near-wake by the formation of Λ-shaped structures and manifests itself in the far-wake as escaping mushroom-type structures from the upper vortices. The legs of these Λ-shaped vortices contain streamwise vorticity generated by baroclinic vorticity production due to the occurring spanwise temperature gradients. These temperature gradients on their turn are linked to the counter-rotating vortices at the rear end of the cylinder.[15] The influence of these near-wake flow phenomena on the vortex shedding process is investigated in Ref. 16. It is shown that quite large differences occur between the different spanwise positions. The formation of the secondary vortical structures in the near-wake is discussed,[17] where a cyclic process is proposed. In the present paper, the three-dimensional transition behind a heated cylinder is investigated with a focus on the development of the Λ-structures toward mushroom-type structures and ultimately toward buoyant vortex rings in the far-wake.

The current investigation focuses on the flow phenomena behind a heated cylinder subjected to a horizontal water flow at one Reynolds number and one Richardson number, Re=85 and Ri=1.0, respectively. In this study, both experimental and numerical techniques are used to investigate the origin and development of these mushroom-type structures, including an electrochemical tin-precipitation visualization method, a combined Laser Induced Fluorescence and Particle Tracking Velocimetry (LIF/PTV) method, and a three-dimensional Spectral Element Method (3D-SEM). The paper is organized as follows. First, a description of the problem definition is given, together with the experimental setup and investigation techniques. Then, the formation and growth process of the mushroom-type structure is investigated and the pinch-off phenomenon is described, separating the stem from the cap. Finally, an analytical model is presented for the pinch-off process.

II. PROBLEM DEFINITION AND SOLUTION METHODS

A. Problem definition

In the current investigation, the cylinder is exposed to a horizontal uniform cross-flow, Fig. 1, where the z axis is in the spanwise direction, the x axis is in the streamwise direction, and the y axis is in the negative gravity direction. The cylinder is positioned at $x=0$ and $y=0$. This paper focuses on the case Re=85, Ri=1.0, and Pr=7, with Reynolds, Richardson, and Prandtl defined as, respectively,

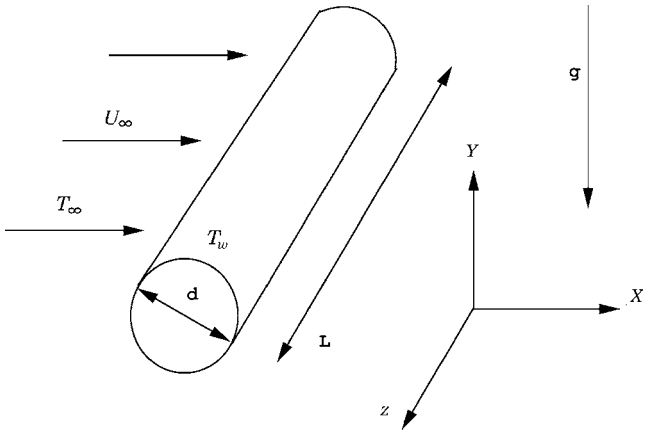

FIG. 1. Problem definition: the cylinder, positioned at $x=0$ and $y=0$, has a temperature T_w and is subject to a horizontal cross-flow with velocity U_∞ and temperature T_∞ and gravity is in the negative y direction.

$$\mathrm{Re} = \frac{U_\infty d}{\nu}, \quad \mathrm{Ri} = \frac{Gr}{\mathrm{Re}^2} = \frac{g\beta(T_w - T_\infty)d}{U_\infty^2}, \quad \mathrm{Pr} = \frac{\nu}{\kappa}. \qquad (1)$$

Here, U_∞ is the main stream velocity, d is the cylinder diameter, ν is the kinematic viscosity, g is the gravity acceleration, β is the thermal expansion coefficient, κ is the thermal diffusivity, and $(T_w - T_\infty)$ is the temperature difference between the cylinder wall and the main stream. In the current investigation, Ri is equal to 1.0 and Re is set to 85, and the corresponding temperature difference is then $(T_w - T_\infty) = 5.7\ ^\circ\mathrm{C}$, using water as the working fluid.

B. Experimental setup

The apparatus used in the experiment consists of three parts: the water tank, the light source with an illumination system, and the image recording with a post-processing system.

The flow is investigated in a so-called towing tank configuration, as shown in Fig. 2, with dimensions length

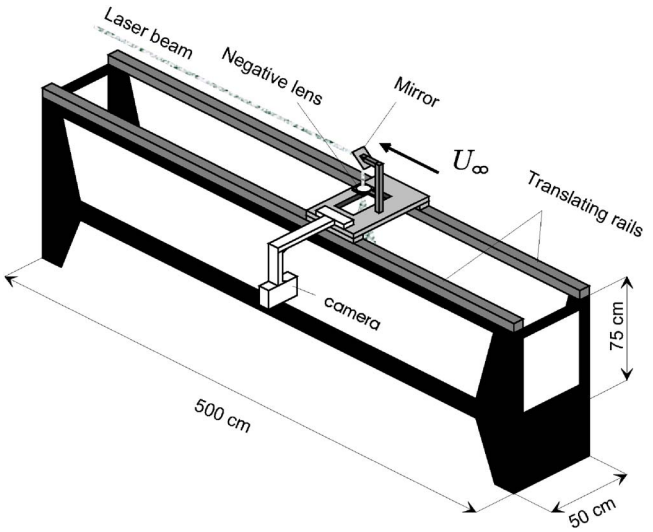

FIG. 2. (Color online) Experimental setup. In this configuration, the cylinder is towed through the water with a constant velocity U_∞.

$\times$ width $\times$ height $=500\times50\times75$ cm^3. In this configuration, the cylinder is towed through the water with a constant velocity U_∞. The cylinder has length $L=495$ mm and diameter $d=8.5$ mm (aspect ratio $L/d=58$). The test section consists of 15 mm thick glass windows, held together by a steel frame, so the towing tank is optically accessible from all directions. The cylinder is positioned between two perspex plates, which are connected to a stiff structure, which also carries measurement equipment such as cameras and light sources. The stiff construction can be translated along two rails that are mounted on top of the water tank. The perspex plates are constructed in such a way that minimum disturbances are created and oblique vortex shedding is suppressed. Parallel shedding is promoted by angling the end plates until the resulting shedding frequency matches the value over the rest of the span of the cylinder.[4]

A cylindrical heating element with diameter 6.35 mm is used to obtain the desired cylinder wall temperature. The whole of the tank is supported by a sturdy steel framework and is situated in a temperature-controlled laboratory. Special care is taken to minimize thermally induced background flows, so most of the experiments show parallel vortex shedding. A detailed description of the towing tank is given in Refs. 18 and 19.

For the light source, a pulsed neodymium:yttrium-aluminum-garnet (Nd:YAG) laser is used. The laser emits light with a wavelength of 532 nm. One laser pulse has a duration of 6 ns and a maximum energy of 200 mJ. The laser beam is directed parallel to the bottom of the water tank, as shown in Fig. 2. The beam passes a negative lens to form a thin laser sheet. The laser is triggered by a camera and operates at 29 Hz. The recording is performed by a CCD camera (Kodak Megaplus, 10-bit ES 1.0, 1008×1019 pixels^2). A Nikon lens with a focal distance of 50 cm is used in front of the CCD camera. A detailed description of the image recording and postprocessing system is given in Refs. 18 and 19.

C. Investigation methods

1. Visualization method

Flow visualizations are carried out using an electrochemical tin-precipitation method (Honji *et al.*[20]). In this method, tin ions are separated from an anode by applying a voltage difference. A thin tin wire, which is used as an anode in the current setup, is positioned upstream of the cylinder. Because the tin ions do not dissolve in pH-neutral water, the small tin-hydroxide particles of $\mathcal{O}(1\ \mu\text{m})$ form a homogeneous sheet that moves toward the cylinder. With this sheet, the wake behind the cylinder is visualized. A detailed description of the visualization method is presented in Ref. 21.

2. Combined LIF/PTV

A reconstruction of the velocity and temperature fields in a 2D plane is performed using a combined Laser Induced Fluorescence (LIF) and Particle Tracking Velocimetry (PTV) method. In order to measure the velocity and temperature fields simultaneously, the tank is seeded with 20 μm hollow spherical particles and fluorescent dye (Rhodamine B with concentration $C_0=1.0\times10^{-4}$mol/m^3).

For the light source, a pulsed Nd:YAG laser is used. The laser emits light with a wavelength of 532 nm. One laser pulse has a duration of 6 ns and a maximum energy of 200 mJ. The laser beam is directed parallel to the cylinder. The beam passes a negative lens and a rectangular diaphragm to form a thin laser sheet.

The light intensity of the laser sheet is recorded with two CCD cameras (Kodak Megaplus, 10-bit ES 1.0, 1008×1019 pixels^2). One camera records the light scattered by the particles filtered with a narrowband pass filter (notch filter with around 10 nm bandwidth) and another one records the fluorescent light reemitted by the Rhodamine B, filtered with a high-pass filter (holographic notch filter: 0% transmission for $\lambda=532$ nm and 80% transmission for $\lambda=575$ nm). Two Nikon lenses with a focal distance of 55 cm are used in front of the CCD cameras. A detailed description of the image recording and postprocessing system is given in Ref. 14. The images are directly stored on two computers using the acquisition software VideoSavant. The laser triggers the cameras in order to synchronize the two cameras and the laser and operates at 30 Hz. More information about this combined measurement technique can be found in Ref. 19.

3. 3D spectral element method

Because of the small temperature differences in the experiment, in the calculations the flow is assumed to obey the Boussinesq approximation. For an efficient temporal discretization of the conservation equations, a splitting operation on the convection-diffusion equations is applied.[22] For the momentum equation, in combination with the continuity equation, a pressure correction method is applied. This results then in three steps, which account for the convection, diffusion, and pressure terms, respectively. The convection equation is integrated forward in time by an explicit third-order Taylor-Galerkin scheme, which is comprised of three explicit time steps within one implicit time step. The diffusion equation is discretized by an implicit second-order backwards difference scheme. The pressure term is treated by a projection method.[23] Due to the limitation of memory storage, an iterative technique is used and the linear system is solved based on a preconditioning conjugate gradient method. The energy equation is solved in a similar way.

For the spatial discretization, a high-order Spectral Element Method (SEM) is used (Karniadakis and Triantafyllou,[24] Dauchy *et al.*[25]). Within an element, the equations are discretized using high-order approximation functions. In this way, a spectral convergence rate and small numerical errors, such as numerical dispersion and diffusion, can be achieved. More information on the validation of the numerical scheme can be found in Ref. 23.

The boundary conditions are prescribed as follows. At the inlet and cylinder wall, Dirichlet boundary conditions are applied for all velocity components and the temperature. The normal velocity and the tangential stresses at the side, top, and bottom walls are set to zero. Also the temperature is set to zero here. At the domain outlet, homogeneous Neumann conditions are prescribed for the normal and tangential velocity components as well as for the temperature. The bound-

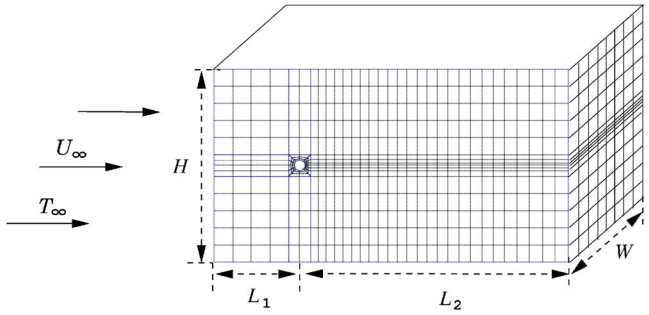

FIG. 3. (Color online) Spectral element grid with dimensions length $\times$ height $\times$ width $=33d\times18d\times4d$ ($L_1=8$ and $L_2=25d$, $H=18d$, and $W=4d$), consisting of 1880 elements and 252315 node points (fifth-order approximation polynomial per element).

ary conditions for the pressure correction follow immediately from the global mass conservation. This implicitly states that the pressure is near zero at the outflow boundary.[23] It should be noticed that the vortices leaving the computational domain will be influenced by the applied boundary condition at the outflow boundary. However, van de Vosse *et al.*[26] showed that this influence is hardly noticeable.

The element distribution used in the calculation is shown in Fig. 3. The calculation dimensions are chosen such that the three-dimensional transition can occur similar to the one found in the experiments, that the blockage effect is minimal, and that the outflow boundary conditions do not influence the near-wake and far-wake behavior ($W=4d$, $H=18d$, $L_1=8d$, and $L_2=25d$). Details about the validation can be found in Ref. 19. Moreover, the experiments and calculations have been quantitatively compared in Ref. 16. There, a good agreement has been achieved between the experimentally measured and numerically calculated velocity fields in the (X-Y) plane at "in-plume" (spanwise position where the plume escapes downstream) and "out-of-plume" (spanwise position where no plume escapes downstream) positions, validating the numerical approach. More detailed information about the numerical method used and validation of the numerical code can be found in Ref. 19.

Proper identification and extraction of vortical structures are important in understanding their origin and dynamics. Here a λ_2 definition is used to represent the topology and geometry of vortex cores. A detailed description of the λ_2 definition can be found in Ref. 27.

III. THE INITIATION PROCESS OF THE MUSHROOM-TYPE STRUCTURES

For Ri=0, the wake flow manifests itself as the von Kármán vortex street, as shown in Fig. 4(a). The tinned anode plate was positioned in such a way that the visualization sheet moved through the upper boundary layer of the cylinder.[21] If one increases the heat input, for Ri=1.0, a three-dimensional transition occurs, which manifests itself in the form of "mushroom-type" structures, as shown in Fig. 4(b). It is observed that these mushroom-type structures escape from the upper vortex and stretches in the negative gravity direction.

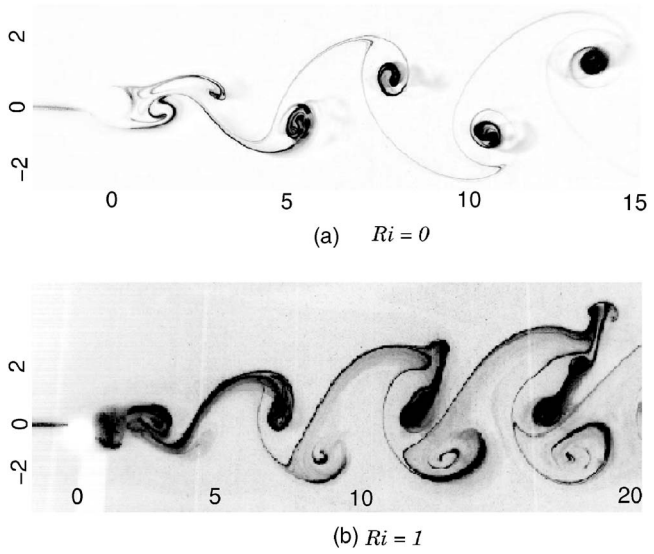

FIG. 4. Side view of the wake flow obtained by tin-precipitation visualization at Re=117 and different Richardson numbers. The flow is from left to right and gravity direction is in the negative y direction (enhanced online).

To get a first impression of the occurring structures, the whole volume behind the heated cylinder was illuminated. The camera was positioned above the cylinder (with some angle with respect to the gravity vector), and the top view of the wake pattern is shown in Fig. 5. For Ri=0, the vortex shedding is two-dimensional. The primary cores of the shed vortices are parallel to the cylinder, as shown in Fig. 5(a). For Ri=1.0, the mushroom-type structures escape from the upper vortices. The spanwise distance between the mushroom-type structures, observed by a top-view visualization, is found to be around twice the cylinder diameter; see Fig. 5(b). The visualizations for different Richardson values at Re=102 and Re=75 showed the same behavior as for Re=117, although the Richardson numbers at which the phenomena start and the quantitative measures may be different.

From the visualizations, it appears that the flow becomes three-dimensional far before the mushroom-type structures escape from the vortices. The three-dimensionality even seems to trace back to the cylinder, which can be seen in Fig.

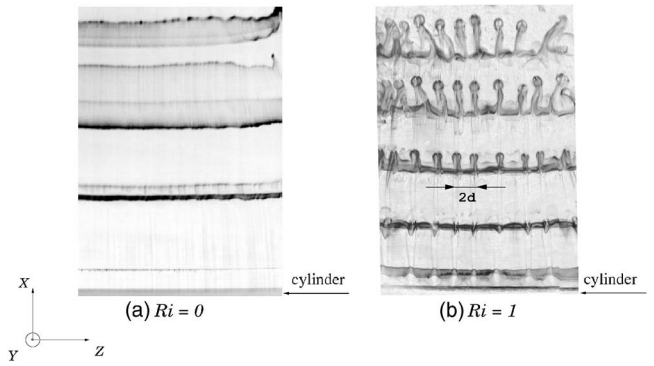

FIG. 5. Top view of the wake flow pattern obtained by tin-precipitation visualization at Re=117 and different Richardson numbers. The flow is from bottom to top and the gravity direction is in the negative y direction. The x-z scales are more or less the same.

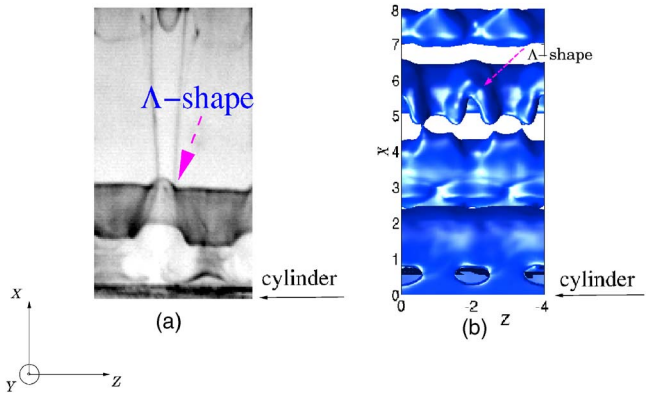

FIG. 6. (Color online) Top view of the wake flow pattern (a) obtained by tin-precipitation visualization at Re=117 and Ri=1.0 and (b) calculated iso-λ_2 surface $\lambda_2=-0.05$ at Re=85 and Ri=1.0. The flow is from bottom to top and the gravity direction is in the negative y direction.

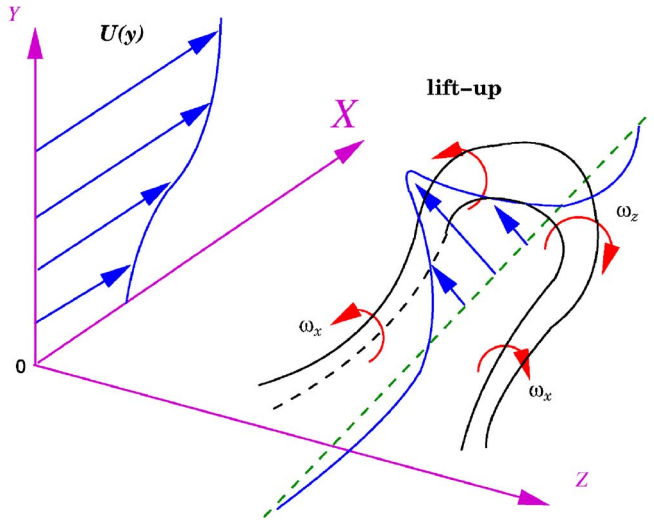

FIG. 7. (Color online) Sketch of the lift-up process initiated by the Λ-shaped structure.[15]

5(b). From this figure it can be concluded that the spanwise positions, at which further downstream the mushroom-type structures are formed, are already determined at the rear end of the cylinder.

Figure 6(a) is a zoom-in picture of a Λ-shaped structure at the rear end of the cylinder obtained by visualization. Figure 6(b) shows the same structure by using the numerically calculated iso-λ_2 surface $\lambda_2=-0.05$. In the near-wake, Λ-shaped structures are observed at $x=5.5$ and the Λ-shaped structures consist of two legs and a head, which is similar to the "hairpin" or "horseshoe" structures observed in boundary layer transition. A schematic of the Λ-shaped structure is presented in Fig. 7. It is known that the Λ-shaped structure is accompanied with the occurrence of low-speed streaks. Low-momentum fluid is accumulated between the two legs, which contain streamwise vorticity generated by baroclinic vorticity production due to the occurring spanwise temperature gradients. These temperature gradients on their turn are linked to the counter-rotating vortices at the rear end of the cylinder.[15] The formation of the secondary vortical structures in the near-wake is discussed,[17] where a cyclic process is proposed. The present paper focuses on the development of the Λ-shaped vortices toward the escaping mushroom-type structures.

The lift-up process between the streamwise legs is essential in the initiation process of the mushroom-type structures, as sketched in Fig. 7. More quantitative experimental evidence of the lift-up process is shown in Fig. 8, where the results are presented of combined temperature and velocity measurements in a vertical plane parallel to the cylinder at position $x=5.0$ for Re=85 and Ri=2.5. From the temperature measurement, a thin "stem" is observed, as indicated in Fig. 8(a). A "cap" shape region is connected with the upper vortex core through this stem. Similar flow structures have been found in numerically calculated results.[15] Counter-rotating vortices (indicated as CRV^x) are observed in the velocity field located around the stem, Fig. 8(b). These CRV^x are the cross-sectional view of the legs of the Λ-shaped structure. The stem region coincides with the upward motion in the velocity field. It is believed that the appearance of a cap shape indicates the birth of a mushroom-type structure.

IV. THE GROWTH PROCESS OF THE MUSHROOM-TYPE STRUCTURES

A. Buoyant plume

In general, it is known that a vortex ring can be produced by releasing a lighter fluid into a heavier ambient fluid (Turner[28]). The energy is provided by the action of the buoyancy force. Such a ring is, therefore, called a buoyant vortex ring. Turner[28] distinguished two physical situations. The vor-

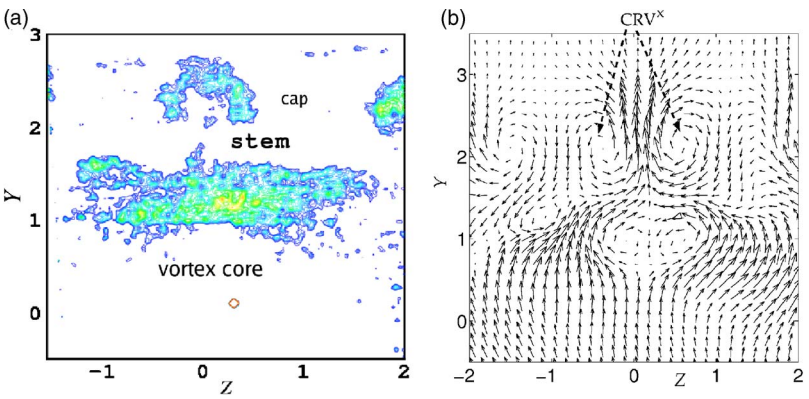

FIG. 8. (Color online) Measured temperature and velocity fields at $x=5.0$ for Re=85 and Ri=2.5 by using a combined LIF/PTV technique. The main flow direction is pointing out of the paper and the gravity direction is in the negative y direction.

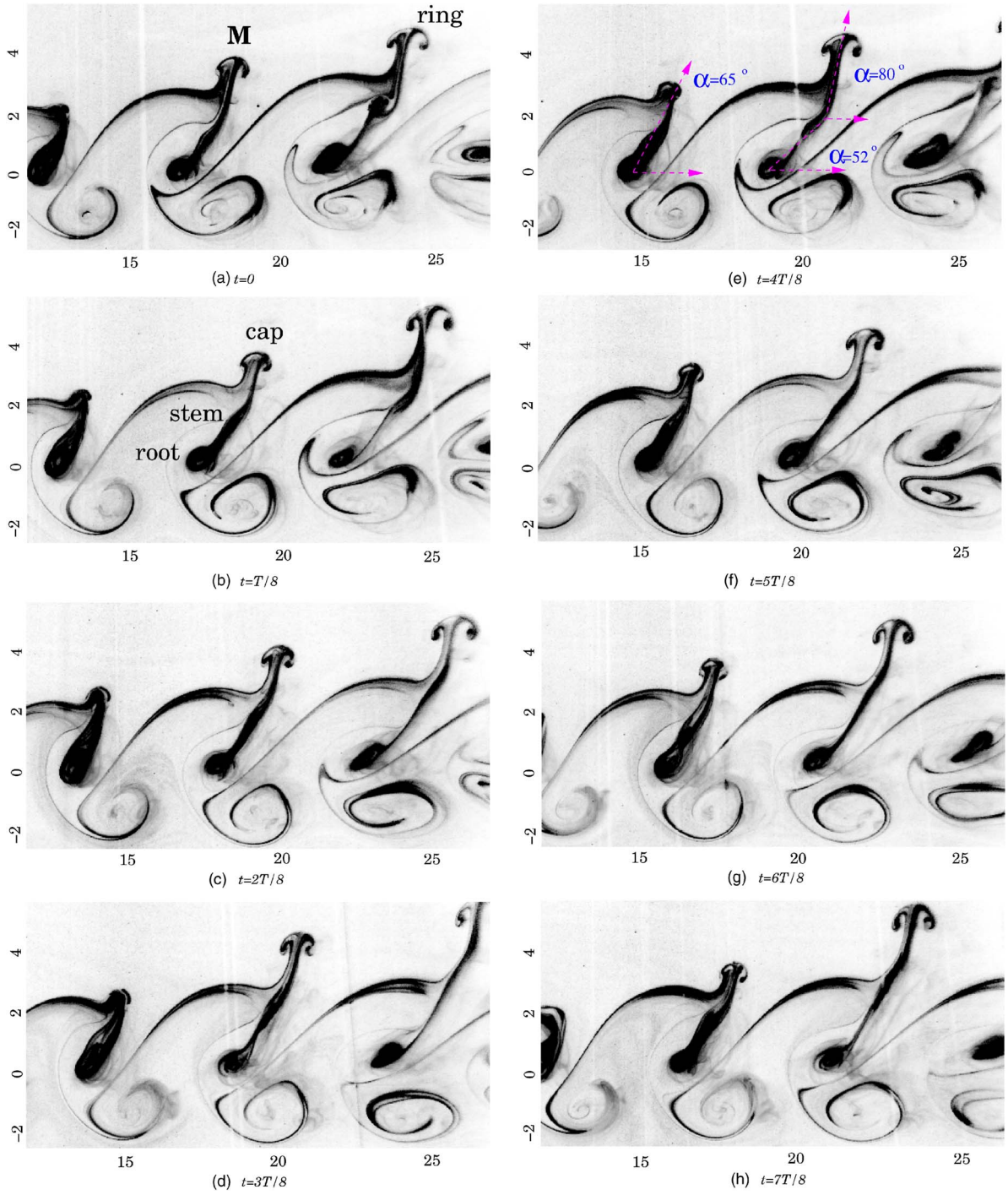

FIG. 9. (Color online) The escape of a thermal plume for Ri=1.0 and Re=117 as shown by visualization. The flow is from left to right and gravity direction is in the negative y direction.

tex ring can be categorized as a starting buoyant plume or a buoyant thermal. The buoyancy supplied steadily from a maintained source generates a starting buoyant plume, while a buoyant thermal is referring to the generation of a ring by a limited volume of hot fluid.

1. Visualization

In Fig. 9, a far wake $(10<x/D<25)$ visualization is shown of the flow at Re=117 and Ri=1.0. The following observations can be made.

First, besides a "cap" at the advancing front, the mushroom-type structure also consists of a "stem" and a "root," as indicated in Fig. 10(b). By definition, the root is located at the vortex core, where the cap originates. The stem is the connection filament between the cap and the root. Such a thin connection was also observed in the temperature measurement; see Fig. 8(a). Through the stem, hot fluid is continuously transported from the vortex core to the cap. Therefore, the current mushroom-type structure is manifested as a starting buoyant plume.

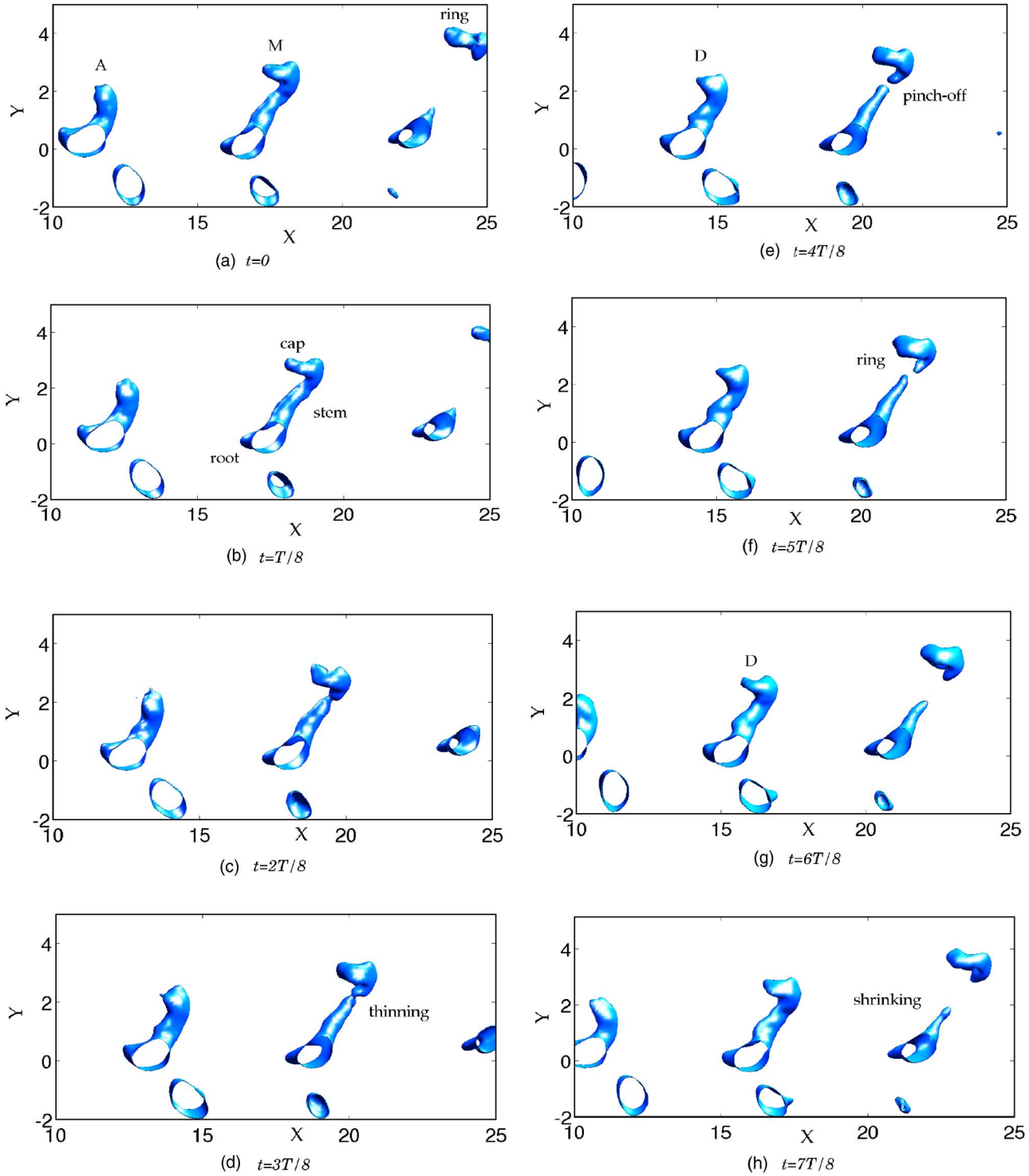

FIG. 10. (Color online) Side view of the numerically calculated flow field $\lambda_2=-0.05$ for Ri=1.0 and Re=85. The flow is from left to right and gravity direction is in the negative y direction.

Secondly, the cap with a radius R_c gradually increases in size as a function of time. Initially, as shown in Fig. 9(a), the cap of the mushroom-type structure is still not visible yet. Gradually, it shows a mushroom shape (M), and in the end it shows a perfect ring shape in the far-wake.

Thirdly, the stem is stretched upwards with time, and this is possibly caused by the continuous addition of buoyancy flux from the vortex core. The stretching of the stem takes place under an inclination angle α, as indicated in Fig. 9(e). This inclination angle varies more or less from $\alpha \simeq 45°$ to $\alpha \simeq 85°$, with an averaged value of $\alpha \simeq 65°$.

This angle of inclination can be compared with experimental observations in boundary-layer studies. Zhou *et al.*[29] found that the tilt angle varies from about 8° in the quasistreamwise legs to about 75° at the downstream end of the hairpin head. A different study by Haidari and Smith[30] re-

ported the angle to vary from about 6° at the upstream portion of the legs to about 67° near the head. But, in general, the average tilt angle is 45° (Head and Bandyopadhyay[31]), which is often quoted in the literature.

It seems that the inclination angle in the current study has the same tendency as the one for a hairpin. However, it is difficult to make such a comparison, because here the buoyancy force plays an important role.

2. Numerical simulation

A numerical simulation is performed to study the evolution of the mushroom-type structure and to compare to the visualization results. Although the types of visualization differ quite a lot (streakline versus λ_2 criterion), the measured and calculated coherent structures reveal some similar patterns, which are quite illustrative. Figure 10 shows the calculated coherent structures by use of iso-λ_2 surface $\lambda_2=-0.05$, for Re=85 and Ri=1.0. From comparison of the results with the visualized flow pattern, the following similarity has been found.

Initially, a mushroom-type structure (M) is observed from both approaches. Strikingly, it is seen that, in Fig. 10(g), a "duck-head" shape (D) is clearly found at the top of the upper vortex. In fact, this phantom corresponds to the shape of a cap (from top view), which symbolizes as the beginning of the mushroom-type structure. Both visualization and calculations show that the mushroom-type structure consists of a "cap," a "stem," and a "root."

In the end, a vortex ring is observed at the cap region in the far-wake, Figs. 10(a) and 9(a). The size of the ring increases with time. Furthermore, calculated inclination angles show the same trend as the visualizations.

B. Formation of vortex ring

Here, a central question is how the vortex ring forms. For this purpose, the calculated spanwise vorticity ω_z is shown in Fig. 11 at the "in-plume" position (spanwise position where the plume escapes downstream). It is found that the duck-head region as found in Fig. 10(e) coincides with an area of positive spanwise vorticity at $x=14$ and $y=2$, indicated with a "+" sign in Fig. 11(d). In other words, the generation of such a positive vorticity area indicates the appearance of the mushroom-type structure.

This area of positive spanwise vorticity (ω_z^+) already exists more upstream, for example at $x=9.0$ and $y=1.7$ in Fig. 11(e). Furthermore, it is seen that ω_z^- is originating from the upper vortex core. Here ω_z^- denotes a region of negative vorticity with a local extreme, which is indicated as "front-strand" (at $y=2$) in Fig. 11(e). The local extreme of ω_z^- has more or less the same order of magnitude as the one in the primary vortex core.

The evolution of both positive and negative spanwise vorticity extremes is studied as a function of time in Fig. 12(a). It is observed that the strength of the positive spanwise vorticity, marked as Δ in Fig. 12(a), steadily increases until it reaches an equilibrium value. However, the strength of ω_z^- gradually decreases with time. In the end, at $x=23.5$ the positive and negative spanwise vorticities have more or less

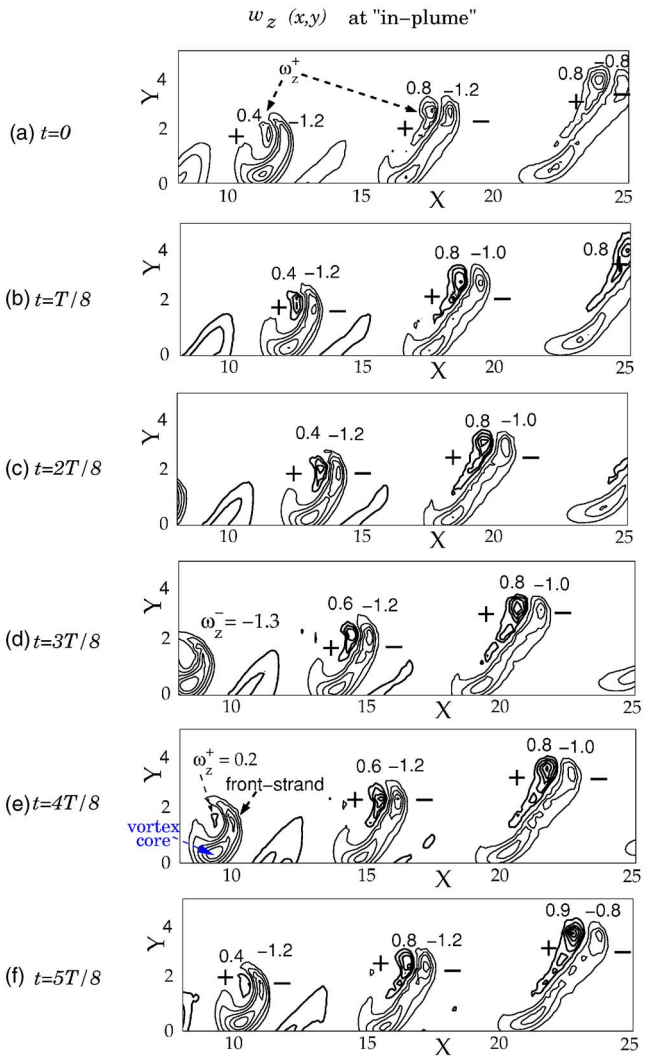

FIG. 11. (Color online) Calculated spanwise vorticity $\omega_z(x,y)$ for Re=85 and Ri=1.0 at the "in-plume" position. The numbers indicate the local maximum values. "+" and "−" are regions with positive and negative spanwise vorticities, respectively. The flow is from left to right and gravity direction is in the negative y direction.

equal strength, $\omega_z^+=|\omega_z^-|=0.9$, and it looks like a "dipole-type" structure. A similar "dipole" structure is also observed from the measured velocity field.[18,12].

With time, the region of the "dipole-type" structure is stretched upwards. The trajectory of the cap/ring is obtained by recording the position of the center of this "dipole-type" structure. Figure 12(b) shows the ring velocity $\mathcal{U}_c$, which steadily increases. Initially, the cap moves slowly upwards, while it accelerates at $t=3.5T$. The acceleration occurs when the strength of positive and negative vorticity reaches more or less the same level; see Fig. 12(a). The reason for this acceleration might be associated with a pinch-off phenomenon, which will be discussed later in this paper.

It is obvious to relate the dipole-like structure to the vorticity generated by baroclinic vorticity production. The presence of the temperature gradients in the x direction gives rise to vorticity production in the z direction, $\Gamma_z=g\mathrm{Ri}\partial\Theta/\partial x$; see Fig. 13. Inside an upper vortex structure, a considerable area of positive (+) and negative (−) vortic-

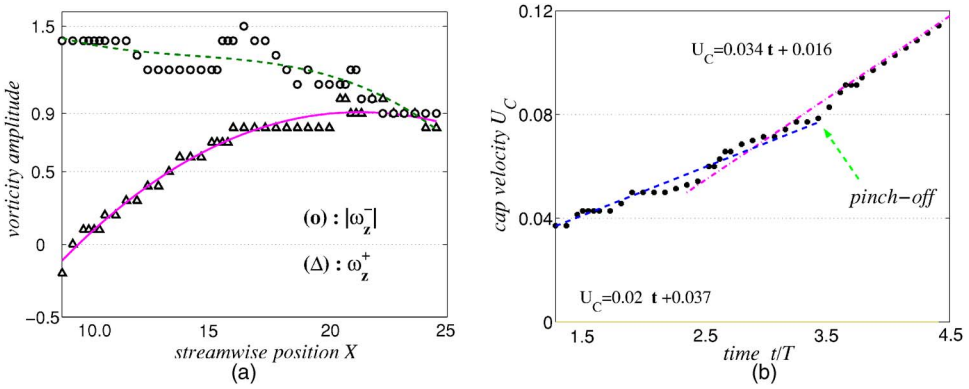

FIG. 12. (Color online) (a) The vorticity extreme of ω_z^+ and $|\omega_z^-|$ as a function of time. The "○" signs indicate positions of the negative vorticity region and "△" signs indicate positions of the positive vorticity region. (b) The cap velocity as a function of time. Note that the scales on the horizontal axis of both figures are interchangeable.

ity production can be found. A closer analysis reveals that the area of positive vorticity production coincides with the developing ω_z^+. This allows us to conclude that the temperature gradients in the x direction are responsible for the growth of positive vorticity, which is located around the cap and the stem.

In general, the area of negative production $(-)$ is found inside the upper vortex and stretched front-strand, as shown in Fig. 13(e). Initially, the production contributes to the growth of ω_z^- and helps vorticity being pulled out of the vortex core. Gradually, the dominance of negative production becomes less because the region experiences a stretching by the buoyancy force.

C. Pinch-off of the vortex ring

It has been shown in Fig. 10(e) that the cap and the vortex core are separated in the end-life stage of the mushroom-type structure. This phenomenon is often quoted as a pinch-off of a vortex ring. Shusser and Gharib[32] showed that when the propagation velocity of the ring becomes equal to or larger than the flow velocity inside the stem, the cap region will be separated from the stem. After the cap separates from the stem, mass flux and energy supply from the stem to the cap is no longer possible. An acceleration of the ring is observed, as shown in Fig. 12(b), soon after the pinch-off. The acceleration can be seen by the change of the slope of the cap velocity $\mathcal{U}_c$. When the stem is separated from the cap, it starts to shrink; see Fig. 10(h). The temperature diffuses very quickly after the pinch-off.

A theoretical model is proposed to associate the acceleration of the cap with the pinch-off phenomenon. Here, the plume is divided into two parts: a stem and a cap. Figure 14 shows the cap located above the stem. Let ρ be the fluid density inside the plume and ρ_A the fluid density outside the plume. The cap velocity $\mathcal{U}_c$ is defined at the center of the cap. Here we assume that the added mass effect, caused by the velocity difference between the cap and the surrounding fluid, is negligible. The impulse $\mathcal{I}$ is proportional to the fluid mass $\mathcal{M}$ within the cap and the cap velocity $\mathcal{U}_c$,

$$\mathcal{I} = \mathcal{M}\mathcal{U}_c. \tag{2}$$

The buoyancy force, which causes the cap to rise, can be formulated as

$$\mathcal{F}_B = (\rho_A - \rho) g \mathcal{V} \tag{3}$$

with $\mathcal{V}$ the volume of the cap. Then, the equation for the cap motion can be written as

$$\frac{d\mathcal{I}}{dt} = \frac{d(\rho \mathcal{V} \mathcal{U}_c)}{dt} = \mathcal{F}_B. \tag{4}$$

The volume of the cap might change by a velocity difference (net mass flux) between the cap and the stem. If the density ρ is taken as constant, Eq. (4) can be rewritten as

$$\rho \mathcal{V} \frac{d\mathcal{U}_c}{dt} + \rho \mathcal{U}_c \frac{d\mathcal{V}}{dt} = (\rho_A - \rho) g \mathcal{V}. \tag{5}$$

Then, an equation for the cap acceleration is derived and reads

$$\frac{d\mathcal{U}_c}{dt} = -\frac{\mathcal{U}_c}{\mathcal{V}} \frac{d\mathcal{V}}{dt} + \left(\frac{\rho_A - \rho}{\rho} \right) g = \mathcal{H}(t) + (\mu - 1) g \tag{6}$$

with $\mathcal{V}$ the volume of the cap and $\mu = \rho_A / \rho$. The second term on the right-hand side,

$$(\mu - 1) g > 0 \quad \text{since } \rho_A > \rho. \tag{7}$$

It is obvious that the motion of the cap depends on the property of the first term $\mathcal{H}(t)$ on the right-hand side of Eq. (6). For a growing plume, due to the continuous addition of mass through the stem to the cap, the volume of the cap increases with time, resulting in

$$\mathcal{H}(t) = -\frac{\mathcal{U}_c}{\mathcal{V}} \frac{d\mathcal{V}}{dt} < 0 \quad \text{since } \frac{d\mathcal{V}}{dt} > 0. \tag{8}$$

However, after pinch-off of the vortex ring, the volume of the cap remains constant, leading to

$$\mathcal{H}(t) = -\frac{\mathcal{U}_c}{\mathcal{V}} \frac{d\mathcal{V}}{dt} = 0 \quad \text{since } \frac{d\mathcal{V}}{dt} = 0. \tag{9}$$

It is clear that the value of $\mathcal{H}(t)$ changes from negative to zero within a short time. This suggests that the change of volume of the cap leads to an acceleration after pinch-off. Therefore, the cap velocity increases after pinch-off, visualized as a difference slope in Fig. 12(b). However, how the volume of the cap and the associated value of $\mathcal{H}(t)$ exactly changes is still not yet clear. It is possible that other effects

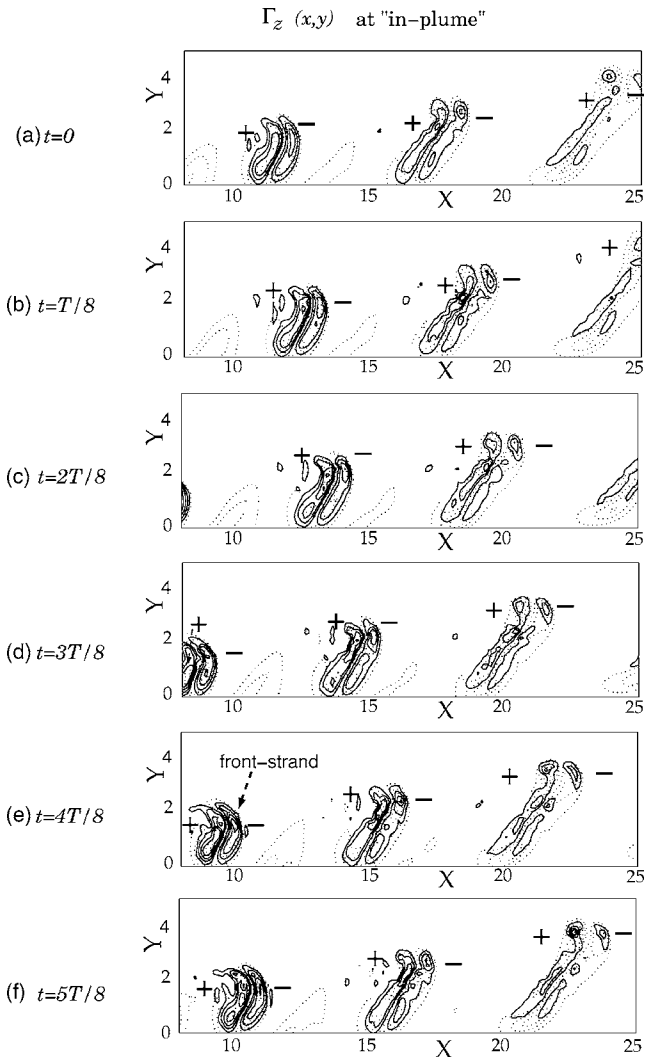

FIG. 13. Calculated baroclinic vorticity production $\Gamma_z(x,y)$ (solid lines) for Re=85 and Ri=1.0 at the "in-plume" position. The dashed lines are the corresponding spanwise vorticity levels $-1.2<\omega_z<0.9$. The "+" and "−" signs indicate regions with positive and negative vorticity production, respectively. The flow is from left to right and gravity is in the negative y direction.

also contribute to the changes in the rising velocity. For example, the relative motion between the cap and displaced ambient fluid might lead to an acceleration of the cap, which is associated with the added mass effect (Landau and Lifshitz[33]). Furthermore, it is also possible that the baroclinic vorticity production induced by density gradients will change the vorticity field surrounding the cap, which in turn influences the cap velocity (Eames and Hunt[34]).

In summary the life of the mushroom-type structure can be described as follows, see Fig. 14. First, hot fluid is lifted up from the vortex core by the action of a Λ-shaped structure. Driven by buoyancy, the Λ-shaped structure is stretched upwards. Secondly, a transition occurs form the Λ-shaped toward mushroom-shape. Hot fluid is transported through the stem to the cap. The mushroom-type structure is characterized by the generation of a vortex ring at the advancing front.

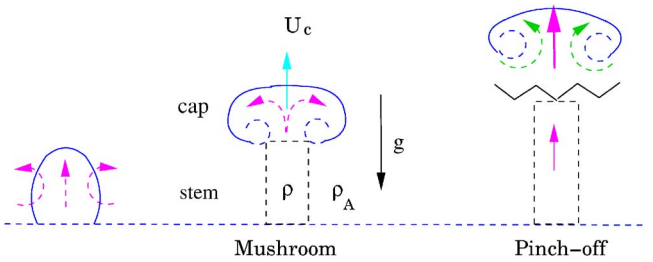

FIG. 14. (Color online) Sketch of formation scenario for the mushroom-type structure.

Finally, a pinch-off phenomenon takes place between the cap and the stem. The cap is separated from the stem and the cap accelerates suddenly, as sketched in Fig. 14(c).

V. SUMMARY AND CONCLUSIONS

It has been shown that the far-wake flow pattern is linked to the coherent structures upstream. Both visualizations and numerical simulations show coherent structures in the near-wake in the form of Λ-shaped structures. The spanwise distance between the Λ-shaped structures is about two cylinder diameters.

Furthermore, escaping mushroom-type structures from the upper vortex cores are observed in the far-wake. The spanwise position of the mushroom-type structures is the same as the one of the Λ-shaped structures. From both experimental and numerical results, the Λ-shaped structures lead to the formation of mushroom-type structures. The route-map for the formation, growth, and pinch-off can be characterized and divided into three phases.

I: The Λ-shaped structure. In this stage, the Λ-shaped structure has been found and consists of two legs and a head. It is observed that the legs coincide with regions of streamwise vorticity. The calculation suggests that the head of the Λ-shaped structure is formed between the legs, due to the fact that part of the vorticity is being pulled out of the primary vortex cores.

II: The lift-up phenomenon. The lift-up process, as sketched in Fig. 7, takes place between the legs and head of the Λ-shaped structure. As a result, hot fluid from the vortex core is transported upwards. Due to buoyancy, which becomes more and more important after the lift-up process, the Λ-shaped structure is transformed into the mushroom-type structure.

III: The mushroom-type structure. The symbolic beginning of the mushroom-type structure is the appearance of a cap, which is a vortex ring forming at the advancing front. The formation of the vortex ring is characterized by the appearance of a region of positive vorticity at the cap region. Additionally, the strength of the positive vorticity increases with time due to baroclinic vorticity production. A pinch-off of the vortex ring is observed when the cap is separated from the stem. The vortex ring accelerates quickly after the pinch-off.

ACKNOWLEDGMENTS

This work is part of the research programs of the Netherlands Foundation for Fundamental Research on Matters (FOM), which is financially supported by the Netherlands Organization for Scientific Research (NWO). The authors appreciate the constructive discussion with Prof. Dr. GertJan van Heijst and technical support from the Laboratory for Energy Technology of the Department of Mechanical Engineering at Eindhoven University of Technology.

[1] C. H. K. Williamson, "Three-dimensional wake transition," J. Fluid Mech. **328**, 345 (1996).
[2] M. Provansal, C. Mathis, and L. Boyer, "Bénard-von Kármán instability: Transient and forced regimes," J. Fluid Mech. **182**, 1 (1987).
[3] C. H. K. Williamson, "The existence of two stages in the transition to three-dimensionality of a cylinder wake," Phys. Fluids **31**, 3165 (1988).
[4] C. H. K. Williamson, "The natural and forced formation of spot-like 'vortex dislocations' in the transition of a wake," J. Fluid Mech. **243**, 393 (1992).
[5] H. Zhang, U. Fey, B. R. Noack, M. König, and H. Eckelmann, "On the transition of cylinder wake," Phys. Fluids **7**, 779 (1995).
[6] N. Michaux-Leblond and M. Bélorgey, "Near-wake behavior of a heated circular cylinder: Viscosity-buoyancy duality," Exp. Therm. Fluid Sci. **15**, 91 (1997).
[7] K. Chang and J. Sa, "The effect of buoyancy on vortex shedding in the near wake of a circular cylinder," J. Fluid Mech. **220**, 253 (1990).
[8] K. Hatanaka and M. Kawahara, "A numerical study of vortex shedding around a heated/cooled circular cylinder by the three-step Taylor-Galerkin method," Int. J. Numer. Methods Fluids **21**, 857 (1995).
[9] J. Mi and R. Antonia, "Temperature distribution within vortices in the wake of a cylinder," Int. J. Heat Mass Transfer **37**, 1048 (1994).
[10] A. Ezersky and D. Ermoshin, "The instability of density stratified vortices," Eur. J. Mech. B/Fluids **14**, 617 (1995).
[11] A. A. van Steenhoven and C. C. M. Rindt, "Flow transition behind a heated cylinder," Int. J. Heat Fluid Flow **24**, 322 (2003).
[12] R. N. Kieft, C. C. M. Rindt, and A. A. van Steenhoven, "Heat induced transition of a stable vortex street," Int. J. Heat Mass Transfer **45**, 2739 (2002).
[13] R. N. Kieft, C. C. M. Rindt, A. A. van Steenhoven, and G. J. F. van Heijst, "On the wake structure behind a heated horizontal cylinder in cross-flow," J. Fluid Mech. **486**, 189 (2003).
[14] M. Ren, C. C. M. Rindt, and A. A. van Steenhoven, "3D vortices in the wake flow behind a heated cylinder," Int. J. Transp. Phenom. **6**, 177 (2004).
[15] M. Ren, C. C. M. Rindt, and A. A. van Steenhoven, "Lift-up process in a heated-cylinder wake flow," Phys. Fluids **18**, 014106 (2006).
[16] M. Ren, C. C. M. Rindt, and A. A. van Steenhoven, "Experimental and numerical investigation of the vortex formation process behind a heated cylinder," Phys. Fluids **16**, 3103 (2004).
[17] M. Ren, C. C. M. Rindt, and A. A. van Steenhoven, "3D transition of a water flow around a heated cylinder at Re=85 and Ri=1.0," J. Fluid Mech. **566**, 195 (2006).
[18] R. N. Kieft, "Mixed convection behind a heated cylinder," Ph.D. thesis, Eindhoven University of Technology, Eindhoven, The Netherlands (2000).
[19] M. Ren, "3D flow transition behind a heated cylinder," Ph.D. thesis, Eindhoven University of Technology, Eindhoven, The Netherlands (2005).
[20] H. Honji, S. Taneda, and M. Tatasuno, "Some practical details of the electrolytic precipitation method of flow visualization," Rep. Res. Inst. Appl. Mech. (Kyushu Univ.) **28**, 83 (1980).
[21] W. J. P. M. Maas, C. C. M. Rindt, and A. A. van Steenhoven, "The influence of heat on the 3D-transition of the Von Kármán–Vortex street," Int. J. Heat Mass Transfer **46**, 3069 (2003).
[22] Y. Maday, A. Patrta, and E. Ronquist, "An operator-integration-factor splitting method for time-dependent problems: Applications to compressible flow," J. Sci. Comput. **5**, 263 (1990).
[23] L. J. P. Timmermans, P. D. Minev, and F. N. van de Vosse, "An approximate projection scheme for incompressible flow using spectral elements," Int. J. Numer. Methods Fluids **22**, 673 (1996).
[24] G. E. Karniadakis and G. S. Triantafyllou, "Three-dimensional dynamics and transition to turbulence in the wake of bluff bodies," J. Fluid Mech. **238**, 1 (1992).
[25] C. Dauchy, J. Dusek, and P. Fraunié, "Primary and secondary instabilities in the wake of a cylinder with free ends," J. Fluid Mech. **332**, 295 (1997).
[26] F. N. van de Vosse, P. D. Minev, and L. J. P. Timmermans, "A spectral element projection scheme for incompressible flow with application to shear-layer stability studies," Houst. J. Math **34**, 295 (1995).
[27] J. Joeng and F. Hussain, "On the identification of a vortex," J. Fluid Mech. **285**, 69 (1995).
[28] J. S. Turner, *Buoyant Effects in Fluids* (Cambridge University Press, Cambridge, UK, 1973).
[29] J. Zhou, R. J. Adrian, S. Balachandar, and T. M. Kendall, "Mechanisms for generating coherent packets of hairpin vortices in channel flow," J. Fluid Mech. **387**, 353 (1999).
[30] A. H. Haidari and C. R. Smith, "The generation and regeneration of single hairpin vortices," J. Fluid Mech. **277**, 135 (1994).
[31] M. R. Head and P. Bandyopadhyay, "New aspects of turbulent boundary layer structure," J. Fluid Mech. **107**, 297 (1981).
[32] M. Shusser and M. Gharib, "A model for vortex ring formation in starting buoyant plume," J. Fluid Mech. **416**, 173 (2000).
[33] L. D. Landau and E. M. Lifshitz, *Fluid Mechanics*, 2nd ed. (Pergamon Press, Oxford, 1987).
[34] I. Eames and J. C. R. Hunt, "Inviscid flow around bodies moving in a weak density gradient in the absence of buoyancy effects" J. Fluid Mech. **353**, 331 (1997).